中国激光

轻量型感知激光雷达关键技术发展综述

李小路[*]，周依尔，毕腾飞，余瑞钦，王子宁，黄建斌，徐立军[**]

北京航空航天大学仪器科学与光电工程学院，北京 100191

摘要　轻量型感知激光雷达(LiDAR)是一种具有环境目标感知能力的主动式三维光学成像技术，在深空探测与无人驾驶领域被广泛应用。回顾了轻量型感知激光雷达关键技术的重要进展，总结了以收发系统和扫描机构为核心的轻量型系统设计，梳理了高精度测距技术和指向误差校正技术的标志性成果，展示了感知激光雷达不同领域的应用，展望了感知激光雷达芯片化、智能化、高性能化的发展趋势。

关键词　成像系统；轻量型感知激光雷达；系统设计；测距精度；指向精度；无人驾驶；深空探测

中图分类号　TN958.98　　　　**文献标志码**　A　　　　　　　　　　**DOI**：10.3788/CJL202249.1910002

1　引　　言

　　轻量型感知激光雷达（LiDAR）是一种用于目标实时感知的三维成像传感器。感知激光雷达搭载于车辆、飞行器等载荷平台，可对环境信息进行实时捕获、采集与处理，为环境目标检测、识别与载荷平台执行决策提供实时精准的数据。与传统测绘型激光雷达相比，感知激光雷达体积小、数据量大、传输速率高，具有全天时和高分辨率的三维成像优势。在三维感知的应用需求牵引下，感知激光雷达技术成为未来发展的热点之一。该技术可适应不同领域的需求，例如深空探测与无人驾驶。随着轻量型感知激光雷达的应用场景不断扩大，打破了仅在航天领域使用的局限，民品级别小型化产品快速发展[1-2]。在无人驾驶领域，激光雷达是智能感知系统最关键的配置之一[3]。为了满足小型化和智能化需求，感知激光雷达的关键技术正向着轻量型系统设计方向发展。本文梳理轻量型感知激光雷达的关键技术研究成果，总结感知激光雷达重要应用，呈现该领域的发展态势和全貌，展望关键技术的发展趋势。

2　轻量型设计推动激光雷达朝集成化与全固态化方向发展

　　为了搭载于无人驾驶汽车、航天器、天体着陆器等载荷平台，激光雷达系统设计需要满足紧凑、质量较轻、点云密度高、成像帧率快等要求。针对该需求，感知激光雷达的设计逐渐向着集成化与全固态化发展。核心器件发展方向为激光器半导体集成化、探测器单光子阵列化以及扫描机构全固态化。

　　为了减小激光器尺寸与功耗，激光雷达光源目前以光纤激光器和半导体激光器为主。光纤激光器利用光纤两端的光学镀膜形成谐振腔，具有可靠性高、不受恶劣环境影响、易于小型化等优点，常应用于航空航天领域中。2015 年中国科学院上海光学精密机械研究所将主振功放（MOPA）光纤激光器应用在交会对接激光雷达中，根据目标距离适应性调整激光重复频率与发射功率，重复频率范围为 5~50 kHz[4]。半导体激光器用半导体材料作为工作物质，具有体积小、寿命长、易于单片集成的特点[5]。目前，905 nm 半导体激光器被广泛应用于自动驾驶领域。以 1550 nm 波段为代表的垂直腔面发射激光器（VCSEL）因其穿透能力强、易高频调制和阵列集成等优势[6]，被认为是下一代激光雷达光源的发展趋势。

　　为了在激光雷达系统小尺寸、低功耗的限制下实现微弱信号探测，具备单光子响应能力的高灵敏度探测器成为研究热点。单光子雪崩二极管（SPAD）通过增大雪崩光电二极管（APD）反向偏置电压至超过击穿电压，提高其灵敏度以实现单光子探测。SPAD 的研究主要集中在大面阵阵列技术上[7]，以便实现激光雷达的快速三维成像，如 2021 年索尼研制了图 1(a) 所示的 189 pixel×600 pixel SPAD 阵列探测器，在 117 klx 背景光照条件下可实现帧率 20 frame/s、距离 200 m 的快速成像[8]。由于 SPAD 仅能判断有无光子，无法提供光强信息且易受背景噪声影响，出现了将

多个 SPAD 像素并联，以响应像素个数反映光强信息的探测器，称为硅光电倍增管探测器（SiPM）或多像素光子计数器（MPPC）[9]。2021 年以色列理工学院研制

4 pixel×4 pixel SiPM 探测器，如图 1（b）所示，其每一像素由 100 个 SPAD 并联组成，可由像素输出并联光电流强度反映入射光强[10]。

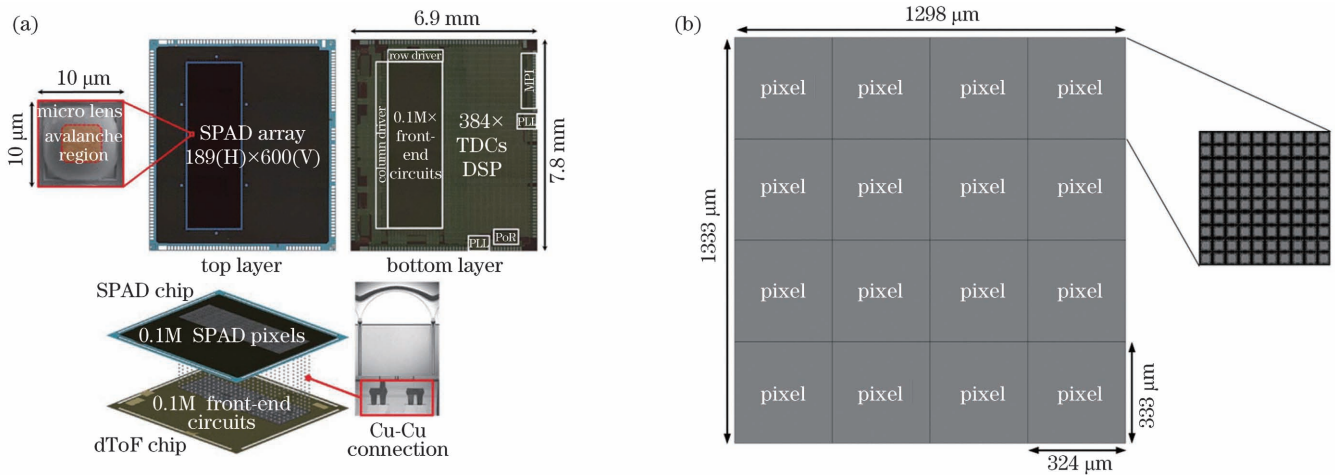图 1　单光子探测器。(a)日本索尼 189 pixel×600 pixel SPAD 阵列[8]；(b)以色列理工学院 4 pixel×4 pixel SiPM 探测器[10]

Fig. 1　Single photon detector. (a) 189 pixel×600 pixel SPAD array by Sony, Japan[8]；(b) 4 pixel×4 pixel SiPM detector by Israel Institute of Technology[10]

为了减小激光雷达系统尺寸、提高扫描速度，多线机械扫描[11]正在逐步被微机电系统（MEMS）和光学相控阵（OPA）替代。MEMS 微振镜是在基底材料上加工出微型反射镜及驱动线圈，通过控制驱动线圈中的电流使微振镜摆动，改变激光指向。当前，MEMS振镜偏转角度小，需要多幅点云拼接实现大范围扫描。2013 年丰田中央研发实验室研发的 MEMS 激光雷达提出了多光束同步收发设计，如图 2（a）所示，通过

MEMS 振镜同时对 3 束出射激光进行扫描，拼接实现45°×11°大范围扫描[12-13]。MEMS 无旋转部件、体积和功耗低、易于集成，但通光孔径较小，覆盖范围小且背景噪声较大[14]。为增大 MEMS 通光孔径，2020 年德国弗劳恩霍夫光子微系统研究所提出同步 MEMS振镜阵列设计，如图 2（b）所示，通过多个 MEMS 振镜的拼接与同步控制，实现 23 mm 等效通光孔径，用于同时对发射与接收光路进行扫描[15]。

图 2　轻量型感知激光雷达扫描技术进展。(a)日本丰田中央研发实验室 MEMS 激光雷达[12]；(b)德国弗劳恩霍夫光子微系统研究所 23 mm 孔径 MEMS 振镜阵列[15]；(c)美国 Analog Photonics OPA 芯片[16]

Fig. 2　Progress in lightweight type-aware LiDAR scanning technology. (a) MEMS LiDAR by Toyota Central R&D Labs, Japan[12]；(b) MEMS scanner array with 23 mm aperture by Fraunhofer Institute for Photonic Microsystems, Germany[15]；(c) OPA chip by Analog Photonics, USA[16]

全固态激光雷达包括 OPA 与 Flash 激光雷达。OPA 激光雷达中，OPA 通过控制各像素单元激光的相位差，合成具有特定方向的主光束，从而实现激光扫描。2019 年美国 Analog Photonics 公司研制了一维 OPA 激光雷达，如图 2（c）所示，其采用的 512 像元 OPA 尺寸为10 mm²，响应时间 30 μs，实现视场角 20°和距离 200 m的点云生成[16]。尽管 OPA 激光雷达无任何活动部件，

结构简单，体积小，扫描速度快[17]，但还存在尚待攻克的难点，包括相位精准控制与集成制造工艺。如能实现旁瓣抑制和扩大扫描范围，相控阵激光雷达前景可期，但从研发到走向成熟直至真正落地仍需时间。

Flash 型激光雷达发射覆盖待测区域的大面积激光，由面阵探测器接收回波，计算探测器阵列中每一像素对应目标的距离，形成目标三维点云。2019 年美国

Advanced Scientific Concepts(ASC)公司研制了用于空间自主交会对接的 Flash 激光雷达,采用 128 pixel×128 pixel InGaAs APD 探测器阵列,探测最远距离为 2 km,成像帧率为 10 Hz[18]。2012 年哈尔滨工业大学研制的 16 pixel×16 pixel Flash 激光雷达[19],以及

2015 年桂林理工大学研制的图 3 所示的 5 pixel×5 pixel Flash 激光雷达,均采用光纤耦合探测器设计,在降低探测器阵列成本的同时增加激光雷达像素数量[20]。目前,国内 Flash 型激光雷达性能受限于高分辨率探测器阵列芯片制造工艺。
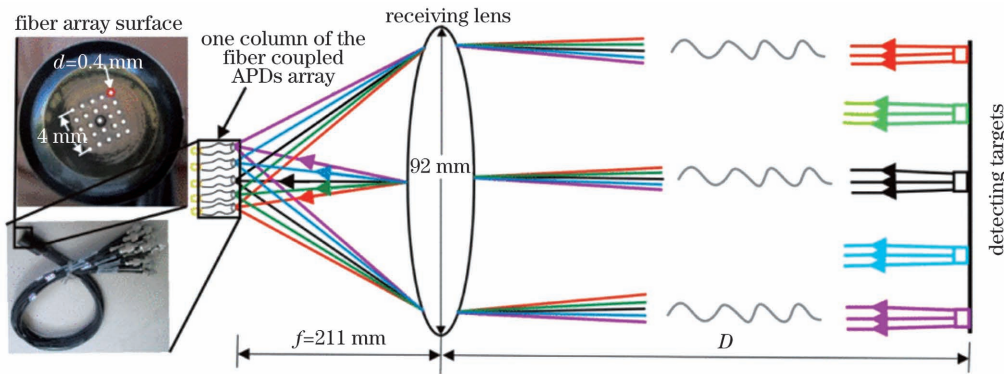

图 3　桂林理工大学 5 pixel×5 pixel 光纤耦合 Flash 激光雷达[20]

Fig. 3　Fiber coupled 5 pixel×5 pixel flash LiDAR by Guilin University of Technology[20]

为了评价系统性能与数据质量,一般从测距、指向、点云三个方面展开评估。激光雷达测距性能可采用测距精确度[21]与精密度作为评价指标,主要受回波质量影响。回波信号质量采用峰值信噪比(PSNR)[22]、混叠度[23]、峰度[24]、偏度[25]和稳定性等指标进行评估。激光雷达指向性能包括视场角范围、角度分辨率、测角误差,受扫描机构和光学接收系统性能影响[26],是影响空间采样分辨率与点云精度的主要因素。点云数据质量主要通过数据率、高程精度、平面精度、点云失真度等指标评估[27-32]。

随着感知激光雷达集成度要求的提高,激光雷达正逐渐从传统多线机械扫描型向 MEMS、OPA、Flash 型激光雷达等多个种类发展,不同类型激光雷达特点及代表性产品如表 1 所示。为进一步提高激光雷达集成度,片上系统(SoC)技术正成为轻量型感知激光雷达的未来发展趋势。SoC 激光雷达是集光电探测、集成电路设计与半导体制造技术为一体的先进制造技术,将依赖于先进半导体材料与半导体制造产业的发展。

表 1　轻量型感知激光雷达扫描机构特点

Table 1　Characteristics of lightweight type-aware LiDAR scanning mechanism

Scanner	Mechanical	MEMS	Flash	OPA
Principle	Mechanical rotation, point by point	Micro-mirror vibrating, point by point	Whole scene with one single laser	Solid-state beam steering, point by point
Advantages	High laser power, long detection range	Ease of integration, mass production	Real time, ease of integration	No moving parts, ease of integration
Drawbacks	Heavy structure	Limited scanning range	High requirements on detector performance	Producing side lobes, leading to large energy loss
Typical products	DJI-TELE 15 (China), Hesai-Pandar (China), Velodyne-VLP (USA), Huawei-96beam (China)	Robosense-M1 (China), Luminar-Iris (USA), Innoviz-Pro (Israel)	Ouster-DF (USA), Ibeo-NEXT (Germany), LuminWave-SMx (China)	Quanergy-S3 (USA), Lumotive-X20 (USA), Litra-LT-X (China)

3　片上系统研发与信号处理算法推动高性能测距技术发展

激光雷达测距性能影响点云成像精度。激光雷达测距模块分为时间-数字转换(TDC)和模拟-数字转换(ADC)两种类型[33]。TDC 测距系统记录发射脉冲和回波脉冲间的参考时钟数,测量两脉冲的时间间隔[34]。该技术测距模式简单、可实时测量目标距离,被广泛应用于多线激光雷达。2021 年,韩国成均馆大学的研究团队针对 SPAD 阵列,设计了 36 通道的

TDC 测距模块,测距范围达 48 m,重复测距精度优于 8.48 mm[35]。2022 年英国格拉斯哥大学在现场可编程门阵列(FPGA)上实现了应用于激光雷达的 128 通道、分离率可调(51.28～105.26 ps)的 TDC 测距技术[36]。然而,TDC 测距技术难以提取单次回波中多个邻近目标的距离[37]。

为了提高测距精度与测距范围,ADC 测距技术采集发射与回波脉冲,通过波形处理算法提取收发时刻。根据波形分解方法,可以实现由单次回波反演多个邻近目标距离。2019 年,奥地利 RIEGL 公司采用 ADC

测距方式设计的激光雷达系统 VZ-400i,在 100 m 处测距精度为 5 mm,且最多可提取单次回波中的 15 个子回波脉冲[38]。但基于 ADC 的全波形测距算法实现复杂,硬件资源与应用成本限制了当前在感知领域中的推广应用[39]。

为了实现激光雷达测距系统的小型化,SoC 正成为激光雷达处理模块的关键技术[40-41],如图 4 所示。相比高速 ADC,TDC 结构简单,在芯片集成过程中占用面积更少、功耗更低,因此,TDC 较早被广泛应用于测距系统的小型化设计。2005 年,瑞士洛桑理工大学(EPFL)研究团队首次在 0.8 μm 互补金属氧化物半导体(CMOS)工艺的基础上实现 32 pixel×32 pixel 的大规模 SPAD 像素阵列,将信号输出至片外 TDC 完成测距等处理。该系统测距精度 1.8 mm,最大测距范围 3 m[42]。为了将探测器阵列和测距电路集成在同一芯片上,2008 年,EPFL 团队采用 32 路并行的 TDC 芯片和 128 pixel×128 pixel 的 SPAD 阵列,实现了首个全集成激光雷达传感器芯片,该系统的测距精度 5.2 mm,最大探测距离 3.75 m[43]。2014 年,EPFL 研究团队采用 TDC 测距模式,结合 SPAD 探测器阵列,设计了像素分辨率为 200 pixel×96 pixel 的片上探测模块,最大探测距离为 100 m,测距精度为探测距离的 0.14%[44]。2019 年,英国爱丁堡大学(Edin.)研究团队研发了一款基于 3D 堆叠技术的 SPAD 激光雷达,该芯片通过混合键合技术将 256 pixel×256 pixel 的 SPAD 阵列和处理电路封装在一起,采用 TDC 测距模式,实现的最远探测距离为 50 m,测距精度约为探测距离的 0.17%[45]。2019 年,荷兰代尔夫特理工大学(TU Delft)研究小组设计了 252 pixel×144 pixel 的 SPAD 阵列激光雷达,该系统包括 1728 个分辨率为 48.8 ps 的 12 位 TDC,可在时间相关单光子计数和单光子计数的模式下工作。该系统的最大探测距离为 50 m,测距精度为探测距离的 0.088%[46]。

为了提升远距离目标的测距精度,TDC 和低采样率 ADC 的混合测距模式被设计使用。2018 年,东芝半导体设计了 20 通道的 TDC 和 ADC 混合模式测距系统,最大探测距离为 200 m,测距精度为探测距离的 0.125%[47]。2020 年,东芝半导体优化 40 通道片上系统,采用双端数据转换器(DDC)在单个电路上集成 ADC 和 TDC,其像素分辨率提高一倍,系统最大探测距离为 225 m,测距精度为探测距离的 0.25%[48]。可以看出,上述技术需要克服探测范围与测距精度两者之间的矛盾。

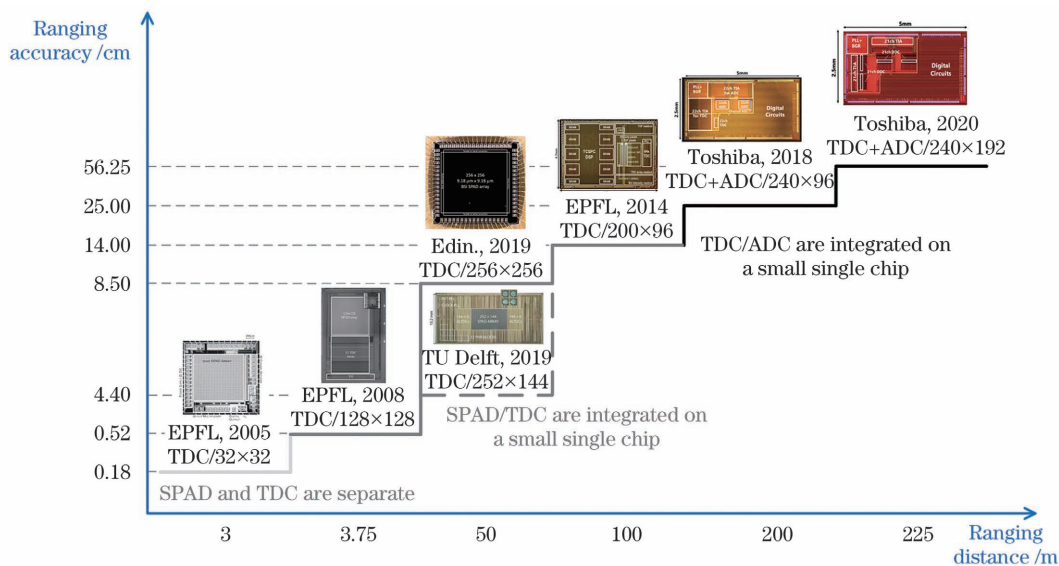图 4 基于 SoC 的阵列激光雷达的性能对比

Fig. 4 Performance comparison of array LiDARs based on SoC

为了提高 ADC 测距模式处理复杂回波信号的能力,研究人员主要针对饱和信号、弱信号和多次回波信号等展开了算法研究。饱和信号是一种激光雷达畸变信号,发生在回波信号幅值高于波形采集单元最大量程的情形下。饱和信号处理算法包括窗宽自适应修正算法[49]和神经网络算法[50]等。2018 年天津大学微电子学院研究团队提出的窗宽自适应修正算法,在波形饱和程度小于 1000% 时,测距精度小于 7.5 cm,但该算法无法获取饱和波形幅值和宽度等信息。2019 年,四川大学 Liu 等[50]对比了 BP 神经网络、Elman 神经网络和径向基函数(RBF)三种网络模型,实验表明 RBF 神经网络对饱和脉冲恢复效果最好。对于激光雷达饱和脉冲信号,由于实际回波波形往往是非对称的,因此研究高精度、高鲁棒性的饱和波形处理算法仍有很大挑战。

弱回波信号表现为回波信号幅值低于部分噪声幅值,一般发生在目标表面反射率过低或系统与目标间的距离过远的情况下。为了提升系统在弱信号时的测距性能,常用的处理算法包括空间域滤波算法[51-55]、时-频域转换滤波算法[56-60]、经验模态分解(EMD)算法[61-65]、变分模态分解(VMD)算法[66-68]、多脉冲相干平均(MCA)算法[69]等。滤波方法的代表性研究成果如表 2 所示。空间域滤波算法采用邻域操作,将固定

滤波模板与输入信号卷积,实现信号滤波。该类算法复杂度低、运行效率高,但参数设置影响滤波效果。空间域滤波算法主要包括高斯滤波[51-52]、Savitzky-Golay 滤波[53-54]、均值滤波等[55]。时-频域转换滤波算法在频域中去除高频噪声,再将频域信号转换到时域。该类方法滤波效果受截止频率选择的影响。时-频域转换滤波算法主要包括基于傅里叶变换的滤波算法[56]

和基于小波变换的滤波算法等[57-60]。通过将若干个弱回波信号进行相干叠加,MCA 算法可进一步提高低信噪比(SNR)回波性能。2019 年,北京航空航天大学研究团队采用 MCA 算法在 20~140 m 测距范围内实现了小于 0.5 mm 的测距误差[69]。通过比较可知,空间域滤波算法和时-频域转换滤波算法运行效率高,可基于 FPGA 实现对回波信号的在线处理。

表 2 滤波算法代表性研究成果

Table 2 Representative research results of filtering algorithms

Filtering method	Characteristics	Representative algorithms	Ref.
Spatial domain	Echo waveform convolved with filtering kernel; high efficiency and real-time filtering; affected by the filtering parameters	Gaussian filtering Savitzky-Golay Average filtering	[51] [54] [55]
Time-frequency domain	Removing high frequency noise in frequency domain; affected by threshold and basis function	Fourier transform Wavelet transform	[56] [57]
EMD	Remaining intrinsic mode functions（IMFs）in time domain; data driven; long execution time	EMD and derivative algorithms	[62,65]
VMD	Remaining IMFs in frequency domain; rigorous mathematical derivation; overcoming modal aliasing; long execution time，affected by the decomposition number K and the quadratic penalty α	VMD and derivative algorithms	[67-68]
MCA	Multiple echo waveforms stacked after shifting and aligning; noise suppression; hard to align signal; increase of heterogenous points	MCA and derivative algorithms	[69]

在处理非线性非平稳信号的技术中,EMD 和 VMD 算法具有性能优势。EMD 算法[61]基于波形特征,将原始信号分解为一系列的固有模态函数(IMF),选取有效的 IMF 对信号进行重构。2021 年 Cheng 等[62]基于改进的 EMD 算法,采用相关系数的差分项准则选取有效 IMF,结合奇异值分解和小波去噪算

法,将回波信号信噪比由 5.28 dB 提升至 21.06 dB。VMD 算法可将信号一次分解为多个有限带宽的调幅-调频函数[66]。2019 年,Hua 等[67]采用 VMD 算法和小波变换滤波算法相结合的方法,将回波信号信噪比由 4 dB 提升至 15.31 dB。EMD 算法和 VMD 算法的滤波效果对比如图5所示。2021年,哈尔滨工业大学
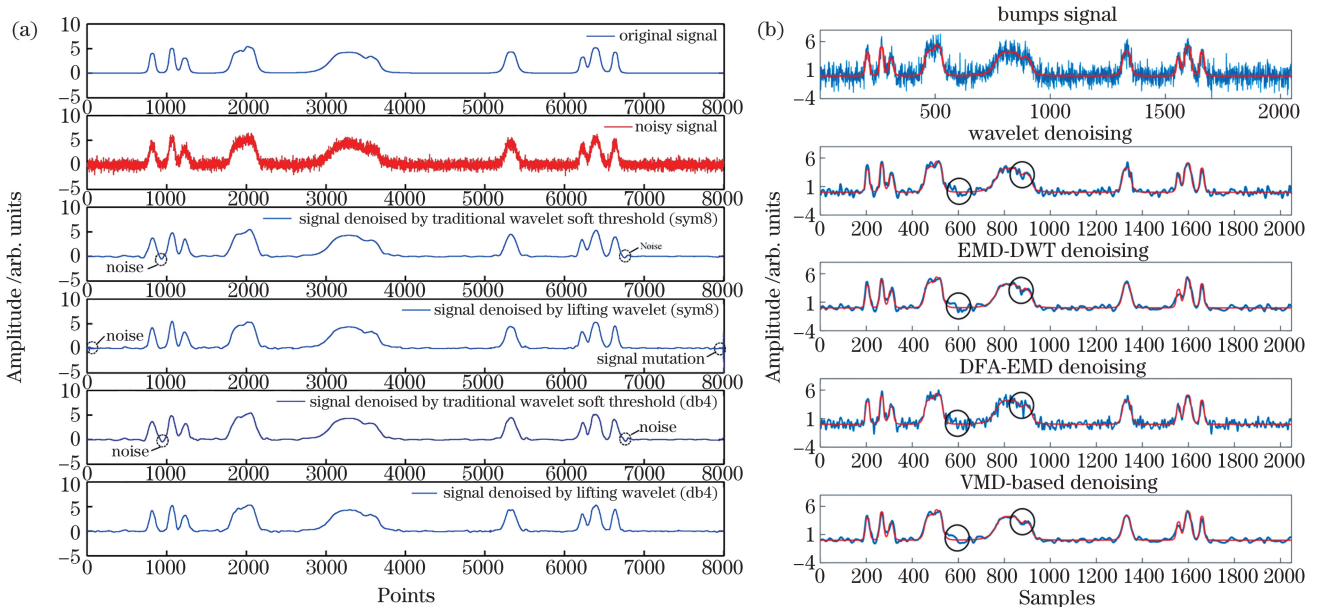

图 5 EMD 和 VMD 算法处理非线性非平稳信号优势对比。(a)不同准则 EMD 算法滤波效果对比[62];(b)EMD 算法与 VMD 算法滤波效果对比[67]

Fig. 5 Superiority of the EMD and VMD algorithms for processing nonlinear and non-stationary signal. (a) Denoising effects of EMD based on different criteria[62]；(b) denoising effects of EMD and VMD[67]

Qi 等[68]采用 EMD 和 VMD 结合的滤波算法,将回波信号信噪比由 4.59 dB 提升至 11.53 dB,且目标探测成功率达 90%。然而,EMD 和 VMD 的滤波算法均需确定信号成分与噪声成分的分界点,当低信噪比引发分界点选取不稳定时,滤波效果将变差[70-72]。

多次回波信号表现为多个子回波叠加后的结果,一般是由于激光传输路径中存在多个测距目标造成的。面向片上系统的测距技术限制,反卷积算法[73-76]、高斯渐进分解法[77-79]等相关算法存在执行时间长的缺点,不适合在线处理。2019 年和 2020 年,北京航空航天大学研究团队基于高斯牛顿法,在 FPGA 上实现了对单脉冲回波信号的在线分解,单次回波信号处理时间提升至 3.5 μs,测距精度为 1.4 cm[41,80]。2021 年,该团队实现了三次回波信号在线分解,测距精度为 1.89 cm[51,54]。目前,在线处理技术主要面临硬件资源和处理速度的平衡问题。

综上所述,不同滤波算法各有其优势和劣势,应根据系统的波形特征与应用需求选取合适的处理算法。感知激光雷达测距技术逐渐向小型化、在线化和低成本的方向发展。其中,为实现感知激光雷达系统的小型化,对目标进行实时探测,SoC 逐渐成为轻量型感知激光雷达测距系统的主流处理形式;处理算法也随着信号复杂度的变化而在不断发展。

4 指向误差校正需要通用化和流程化的技术

感知激光雷达成本低廉。其扫描机构的指向精度是影响点云定位误差的主要因素。感知激光雷达的三维扫描通过旋转机构、振镜或者无扫描体制实现,在不同的方位和俯仰角度引导激光束,从而决定激光束的指向[81-83]。激光束的指向误差对点云定位误差的影响不可忽视,且在远距离探测时易引起较大的点云畸变。因此,国内外学者对指向误差溯源和校正方法展开了研究。

为了实现指向控制机构误差的溯源与校正,研究人员针对不同结构的激光雷达,如棱镜式、MEMS 和 OPA,展开指向误差的研究。2014 年,国防科技大学研究团队基于斯涅尔定律和射线追踪法,发现指向误差来源包括棱镜的楔角误差和折射率误差[84]。2021 年美国佛罗里达大学研究团队针对 Livox Mid-40 棱镜式激光雷达,采用基于最小二乘的平面约束方法,使指向精度提升 94.4%[85]。2021 年哈尔滨工业大学研究团队针对二维 MEMS 振镜的点云视场畸变,提出坐标系归一化计算的校正方法,使目标轮廓的变形程度降低 72.5%[86]。同年,中国科学技术大学研究团队提出基于二乘法的多项式插值标定方法,实现二维扫描畸变的校正,如图 6 所示,校正后图像的二维方向残差小于 4 pixel[87]。

对于 OPA 激光雷达而言,由于加工工艺导致的误差、热光效应及热串扰等因素,易造成相位误差从而影响指向精度。2019 年,澳大利亚国立大学研究团队提出一种数字增强外差干涉技术,实现仅 25.6 mrad 的 OPA 相位误差[88]。2019 年,北京航空航天大学 Zhang 等[89]提出混沌随机并行梯度下降方法,通过优化调制电压实现光束高精度指向。2021 年,吉林大学唐辉[90]基于逐路搜索算法,校准角度波导控制电压或电流,峰值旁瓣电平降低 89.7%。

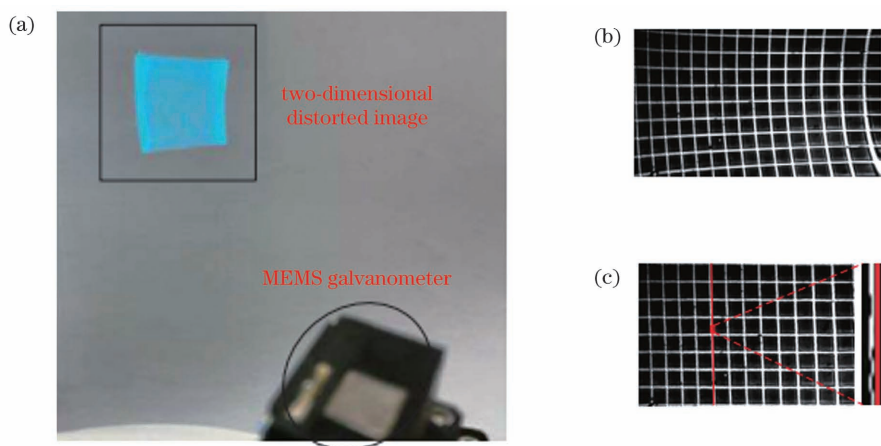
图 6 MEMS 二维振镜扫描的畸变校正与结果[87]。(a)扫描图像;(b)网格测试靶畸变图像;(c)畸变校正后网格图像

Fig. 6 Distortion and correction results of MEMS two-dimensional galvanometer scanning[87]. (a) Actual scanning image; (b) distorted image of grid test target; (c) grid image after distortion correction

除了扫描机构本身带来的点云定位误差,存在的安装误差也会引起点云定位精度的降低。安装误差模型建立的本质是描述实际射线路径和理想路径之间的差值模型[91]。2015 年,美国国家技术研究所基于光线追踪法建立了详尽的安装角度误差模型,包含 18 个误差参数[81]。该安装误差模型为误差求解提供了数学基础。安装误差模型求解的本质是误差估计的优化问题,常用方法包含网络法[92-93]、双面法[94-95]和长度一致法[96]。网络法从不同位置测量相同的目标,使同一目标在其他站点进行坐标转换之后位置尽可能重叠;双面法在网络法的基础上对目标进行正面和背面扫描;长度一致法的优化准则是

从不同位置确定的任何两个目标之间的长度应尽可能接近。2017 年,美国国家技术研究所的 Wang 等[96]提出双面法和长度一致法的自标定校正方法并与网络法比较,校正后的指向角误差如图 7 所示,三

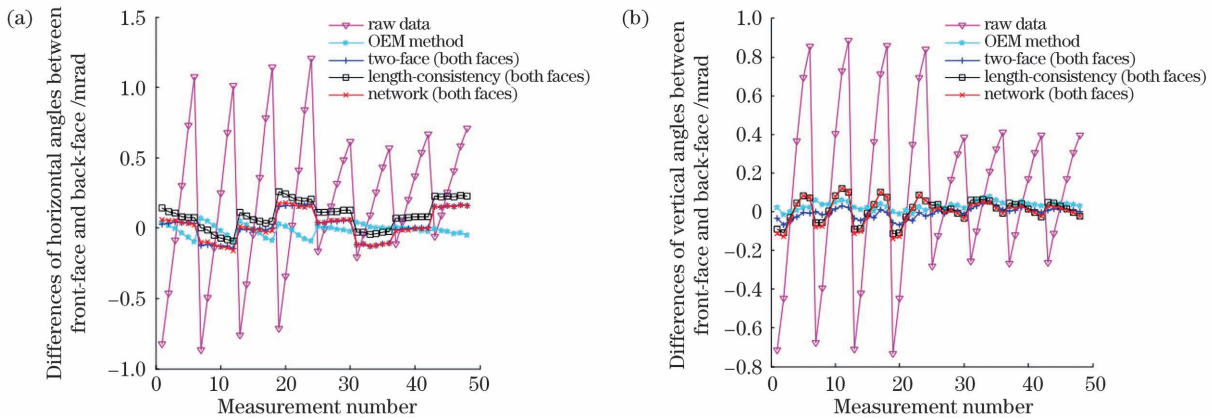种方法分别将指向精度提升 81.5%、75.1% 和 80.8%。当前研究表明轻量型感知激光雷达需要更加灵活的指向误差自校正流程,以提升安装误差标定的灵活性和通用性。

图 7　正面和背面点角度误差曲线图,对比双面法、长度一致法与网络法校正的有效性[96]。(a)水平角度;(b)竖直角度
Fig. 7　Angle errors of the front and back points comparing the effectiveness of the two-face, the length-consistency and the network methods[96]. (a) Horizontal angles; (b) vertical angles

除了模型建立与求解方法,标定目标类型也会影响安装误差标定精度。根据标定目标的类型,自标定方法可分为基于球的自标定方法[97]、基于平面的自标定方法[98-101]和基于圆柱的自标定方法[102]。在标定环境中布局不同形状的目标,构造几何网络,优化安装误差模型,求解标定参数。2014 年东华理工大学研究团队利用球靶标构建了具有 11 个参数的激光扫描仪自检校误差模型,校正后点云定位精度提高 51%[97]。2015 年加拿

大卡尔加里大学研究团队利用圆柱自标定方法,静态数据集和动态数据集的精度分别提高了约 72% 和 41%,其校正步骤如图 8 所示[102]。2020 年天津大学研究团队采用平面自标定方法实现误差标定,使点云定位误差下降 88.6%[98]。总体来看,球靶标自标定方法易导致参数存在耦合相关性,圆柱自标定方法受场景限制,平面自标定方法可操作性更强。未来,激光雷达系统的扫描体制与标定标靶的选择仍是一个值得深入研究的方向。
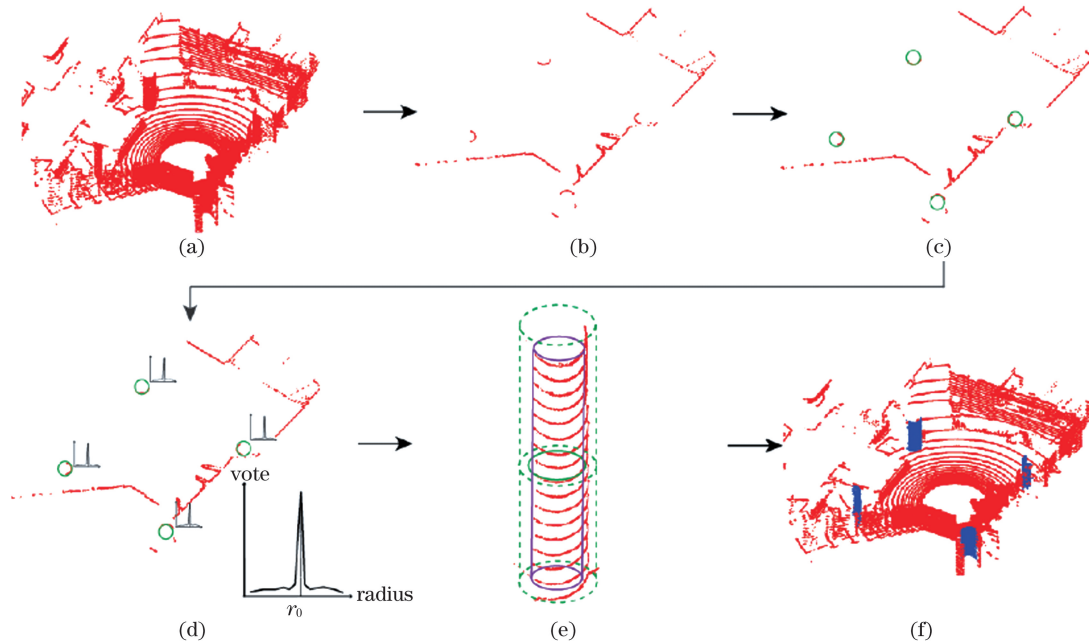
图 8　基于圆柱目标的校正[102]。(a)Velodyne 激光雷达的完整点云;(b)基于分层和密度的点云分割;(c)基于 Hough 变换的二维圆检测(绿色圆圈);(d)半径的直方图统计;(e)圆柱提取(绿色虚线)及基于粗差检测的圆柱体拟合(紫红);(f)分割出的圆柱体(蓝色)
Fig. 8　Calibration based on cylindrical target[102]. (a) The whole Velodyne point cloud; (b) layer and density segmentation; (c) 2D Hough circle detection (green); (d) radius histogram examination; (e) cylinder extraction (green dash) followed by cylinder fitting with blunder detection (magenta); (f) the segmented cylinders (blue)

综上所述,感知激光雷达的点云定位误差主要受到指向精度的影响,指向误差由扫描机构内部机理和系统安装误差引起。扫描机构内部机理的误差通过理论分析所得校正函数进行消除;系统安装误差很难从来源修正,但可通过自校正模型实现误差抑制。由于实际应用场景多变、条件各异,通用化和流程化的误差校正方法尚待继续深入研究。

5 感知激光雷达在民用与航天领域的不断拓展

近年来,随着自动驾驶技术的蓬勃发展,以激光雷达为核心的多传感器融合方案被广泛应用于智能化车型中[103-105]。作为推动自动驾驶跨越 L3 级别的重要条件,激光雷达被搭载于诸多车企的自动驾驶车型中。常用轻量型感知激光雷达产品分类如图 9 所示。机械式激光雷达的测距精度一般为 2~7 cm,探测范围 100~500 m;半固态 MEMS 激光雷达测距精度最高可达 1 cm,探测范围集中在 150~500 m;当前纯固态激光雷达测距精度性能不佳,其中 Flash 激光雷达应用于航天探测领域,探测范围可达 1.8 km,而 OPA 激光雷达探测范围仅为 20 m。尽管 OPA 性能还未达到预期,OPA 纯固态激光雷达无活动部件,具备更高的可靠性、集成度和可控性,还是有望成为未来自动驾驶激光雷达的核心器件[106-108]。
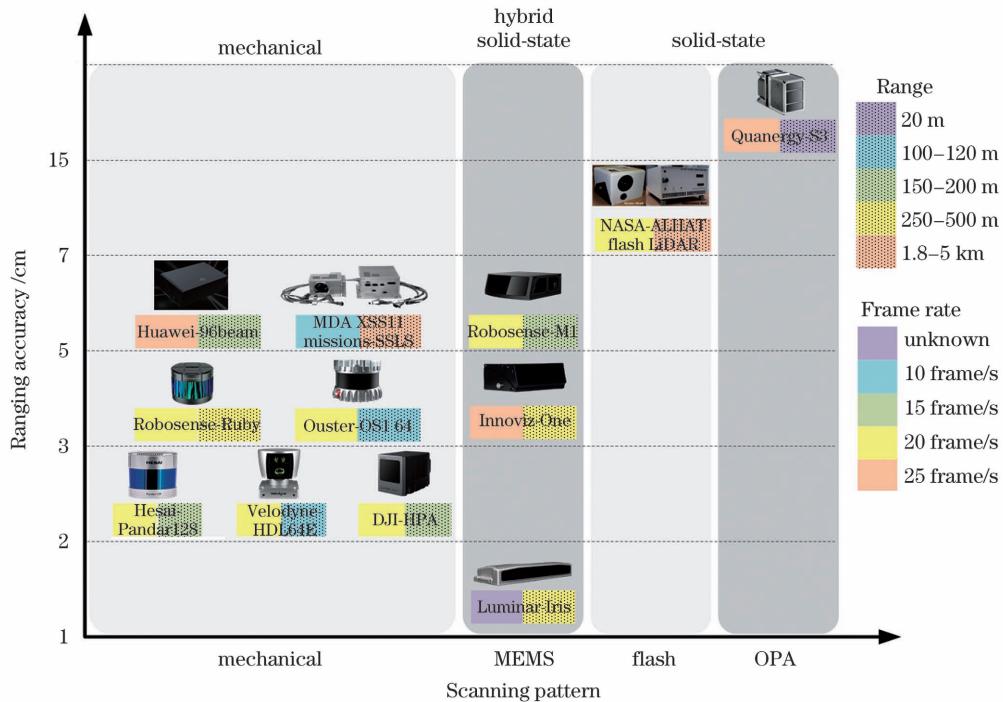

图 9　轻量型感知激光雷达产品分类示意图

Fig. 9　Schematic diagram of classification for lightweight type-aware LiDAR

激光雷达具有高指向性、高分辨率、高精度等优势,常应用于空间交会对接、高精度导航、制导机动避障任务中,相关系统如图 10 所示。近年来,应用于交会对接的激光雷达系统作用范围为几米到几十千米[4,109],国内外交会对接系统发展趋势为高精度、高实时性、多传感器融合[110-115]。空间交会对接激光雷达性能如表 3 所示。Flash 激光雷达因具备快速记录全场景的优势,正逐渐成为交会对接激光雷达系统的主流。2007 年,美国国家航空航天局(NASA)与 Lockheed Martin 公司为猎户座多用途载人飞行器(MPCV)研制了交会对接相对导航系统,搭载的视觉导航系统(VNS)是 256 pixel×256 pixel 的 Flash 激光雷达,视场角可达 20°,实现美国首次自主交会对接[111]。我国首次无人自主交会对接发生于 2011 年神舟八号飞船与天宫一号实验室,其上搭载了微波雷达、激光雷达、电荷耦合器件(CCD)光学成像敏感器等多种测量设备,对接时位置偏差小于 5 cm,相对姿态角偏差小于 0.3°[112]。这些对接敏感器性能随后在天宫一号与神舟九号、神舟十号无人和载人飞船的自动交会对接上得到了进一步验证[113]。

障碍识别、高精度导航和制导机动避障是探测器软着陆涉及的关键技术[116-123]。着陆激光雷达的性能及应用如表 4 所示。2013 年,我国在嫦娥三号探测器上首次采用成像激光雷达实现自主着陆,作用范围为 40~160 m,成像精度为 15 cm,能有效识别障碍,协助探测器选择安全着陆点[117-118]。2014 年,日本隼鸟 2 号(Hayabusa2)小行星探测器上的激光雷达用于估计小行星的地形、重力和地表反射率,成像范围覆盖 30 m~25 km,测距分辨率可达 0.5 m,测距精度为 1 m@30 m 以及 5.5 m@25 km,可指导探测器着陆[119]。

图 10 地外探测领域激光雷达产品。(a)加拿大 XSS-11 星载扫描激光雷达系统[110];(b)中国嫦娥三号激光三维成像仪[118];
(c)日本 Hayabusa2 激光雷达[119];(d)美国 ALHAT Flash 激光雷达[120];(e)美国 OSIRIS 扫描型激光雷达[122]

Fig. 10 LiDAR systems in space exploration. (a) XSS-11 spaceborne scanning LiDAR system[110], Canada; (b) LiDAR system of Chang'e 3[118], China; (c) LiDAR system of Hayabusa2[119], Japan; (d) ALHAT flash LiDAR[120], USA; (e) OSIRIS scanning LiDAR[122], USA

表 3 空间交会对接激光雷达性能

Table 3 LiDAR performance for docking in space

Year	Country	Mission	Payload	Performance	Service time
2005[110]	Canada	—	Experimental Satellite System，XSS-11	Ranging accuracy 5 cm@50 m	2005—2007
2014[111]	USA	Artemis Program	Orion Multi-Purpose Crew Vehicle	Pixel count 256 pixel×256 pixel，field of view 20°	2014—now
2011[113]	China	China Manned Space	Shenzhou-8	Position accuracy <5 cm，attitude accuracy <0.3°	2011.11.01—2011.11.17
2012[114]	USA	—	Dragon	Pixel count 126 pixel×126 pixel，maximum range 750 m	2012.10.08—2012.10.28
2020[115]	China	China's Lunar Exploration Project	Chang'e 5	Range 15 m—20 km	2020.11.24—2020.12.17

表 4 软着陆激光雷达性能

Table 4 LiDAR performance for landing in space

Landing year	Country	Mission	Payload	Performance	Service time
2013[118]	China	China's Lunar Exploration Project	Chang'e 3	Range 40—160 m，accuracy 15 cm	2013—2016
2018[119]	Japan	Hayabusa2	Hayabusa2	Range 30 m—25 km，ranging resolution 0.5 m，ranging accuracy 1 m@30 m	2014—2020
2014[120]	USA	ALHAT	ALHAT probe	Range 500—1000 m，ranging accuracy 8 cm	—
Expected 2024[121]	USA	Europa Lander mission	Europa probe	Pixel count 2000 pixel×2000 pixel，ranging accuracy 5 cm@500 m	—
2018[122]	USA	OSIRIS-Rex	OSIRIS-Rex spacecraft	Maximum range >7.4 km，ranging accuracy <0.5 m	2016—now
2021[123]	China	China's Mars Exploration mission	Tianwen 1	Landing accuracy 3.1 km×0.2 km	2020—now

　　总而言之，因高精度、实时成像等优越性能，轻量型感知激光雷达在自动驾驶、交会对接、探测器着陆等民用与航天领域有着广泛应用。成本是制约商业化激光雷达发展的关键因素，小型化、可批量生产的纯固态式激光雷达正成为民用发展热点；而对于航天领域而言，高精度与实时成像是对激光雷达的关键要求，以 Flash 激光雷达为代表的快速成像三维激光雷达系统正成为航天探测器不可或缺的敏感器。

6　结束语

　　感知激光雷达是智能感知传感器领域的发展前沿与研究热点，随着不同需求涌现出不同分支。近十年来，随着感知激光雷达系统集成化、智能化的发展趋势，我国涌现了以半固态 MEMS 激光雷达为代表的成熟产品，不同产品的最优性能可达到等效 1280 线、测距精度 1 cm。部分技术受限于制造工艺水平，与国外存在一定技术差距，如 Flash 探测阵列和 OPA 芯片。随着集成芯片技术的快速发展，SoC 测距技术或将成为轻量型感知激光雷达系统的主流解决方案，推动激光雷达系统达到芯片级突破。在无人驾驶领域，轻量型感知激光雷达将继续向小型化、低成本、高精度的方向发展，逐步实现规模化应用。在航天应用领域，感知激光雷达具备了高分辨率三维成像优势，将为载人航天、探月工程等国家重大航天任务提供关键技术支持。未来，片上技术配合复杂信号处理算法，新型扫描机构结合通用性指向校正方法，民用与航天领域的相互借鉴、相互推动，都将成为感知激光雷达领域向前发展的创新驱动力。

参 考 文 献

[1] 陈建武, 史永敏, 祝浩, 等. 深空探测中着陆雷达技术发展与应用研究[J]. 航天返回与遥感, 2020, 41(4): 10-20.
Chen J W, Shi Y M, Zhu H, et al. Research on the development and application of landing radar in deep space explorations[J]. Spacecraft Recovery & Remote Sensing, 2020, 41(4): 10-20.

[2] 张海峰, 程志恩, 李朴, 等. 激光雷达合作目标设计及其在空间交会对接中的应用[J]. 红外与激光工程, 2015, 44(9): 2556-2561.
Zhang H F, Cheng Z E, Li P, et al. Design of lidar cooperative target and its application to space rendezvous and docking[J]. Infrared and Laser Engineering, 2015, 44(9): 2556-2561.

[3] 汪阳. 激光雷达行业分析[R]. 香港: 安信国际研究部, 2021.
Wang Y. LiDAR industry analysis[R]. Hongkong: Research Department of Essence International, 2021.

[4] Luo Y, He Y, Gao M, et al. Fiber laser-based scanning lidar for space rendezvous and docking[J]. Applied Optics, 2015, 54(9): 2470-2476.

[5] 宁永强, 陈泳屹, 张俊, 等. 大功率半导体激光器发展及相关技术概述[J]. 光学学报, 2021, 41(1): 0114001.
Ning Y Q, Chen Y Y, Zhang J, et al. Brief review of development and techniques for high power semiconductor lasers[J]. Acta Optica Sinica, 2021, 41(1): 0114001.

[6] 王阳, 崔碧峰, 房天啸. 垂直腔面发射激光器(VCSEL)的研究进展[J]. 光电子, 2017, 7(2): 50-57.
Wang Y, Cui B F, Fang T X. Research progress of VCSEL[J]. Optoelectronics, 2017, 7(2): 50-57.

[7] Aull B F, Duerr E K, Frechette J P, et al. Large-format Geiger-mode avalanche photodiode arrays and readout circuits[J]. IEEE Journal of Selected Topics in Quantum Electronics, 2018, 24(2): 3800510.

[8] Kumagai O, Ohmachi J, Matsumura M, et al. 7.3 A 189×600 back-illuminated stacked SPAD direct time-of-flight depth sensor for automotive LiDAR systems[C]//2021 IEEE International Solid-State Circuits Conference, February 13-22, 2021, San Francisco, CA, USA. New York: IEEE Press, 2021: 110-112.

[9] Agishev R. Modeling of microjoule and millijoule energy LIDARs with PMT/SiPM/APD detectors: a sensitivity analysis[J]. Applied Optics, 2018, 57(14): 3679-3686.

[10] Eshkoli A, Nemirovsky Y. Characterization and architecture of monolithic N'P-CMOS-SiPM array for ToF measurements[J]. IEEE Transactions on Instrumentation and Measurement, 2021, 70: 2002909.

[11] Bohren J, Foote T, Keller J, et al. Little Ben: the Ben Franklin racing team's entry in the 2007 DARPA urban challenge[J]. Journal of Field Robotics, 2008, 25(9): 598-614.

[12] Niclass C, Ito K, Soga M, et al. Design and characterization of a 256×64-pixel single-photon imager in CMOS for a MEMS-based laser scanning time-of-flight sensor[J]. Optics Express, 2012, 20(11): 11863-11881.

[13] Ito K, Niclass C, Aoyagi I, et al. System design and performance characterization of a MEMS-based laser scanning time-of-flight sensor based on a 256×64-pixel single-photon imager[J]. IEEE Photonics Journal, 2013, 5(2): 6800114.

[14] Zhu C X, Hobbs M J, Grainger M P, et al. Design and realization of a wide field of view infrared scanning system with an integrated micro-electromechanical system mirror[J]. Applied Optics, 2018, 57(36): 10449-10457.

[15] Sandner T, Graßhoff T, Owe W D, et al. System integration of hybrid large aperture micro scanner array for fast scanning LiDAR sensors[J]. Proceedings of SPIE, 2020, 11293: 112930Z.

[16] Poulton C V, Byrd M J, Russo P, et al. Long-range LiDAR and free-space data communication with high-performance optical phased arrays[J]. IEEE Journal of Selected Topics in Quantum Electronics, 2019, 25(5): 7700108.

[17] Hsu C P, Li B D, Solano-Rivas B, et al. A review and perspective on optical phased array for automotive LiDAR[J]. IEEE Journal of Selected Topics in Quantum Electronics, 2021, 27(1): 8300416.

[18] Sornsin B A, Short B W, Bourbeau T N, et al. Global shutter solid state flash lidar for spacecraft navigation and docking applications[J]. Proceedings of SPIE, 2019, 11005: 110050W.

[19] 靳辰飞, 王野, 曹璐, 等. 光纤阵列成像激光雷达系统的设计[J]. 光电工程, 2012, 39(11): 115-123.
Jin C F, Wang Y, Cao L, et al. Design of fiber-array imaging laser radar system[J]. Opto-Electronic Engineering, 2012, 39(11): 115-123.

[20] Zhou G Q, Zhou X, Yang J Z, et al. Flash lidar sensor using fiber-coupled APDs[J]. IEEE Sensors Journal, 2015, 15(9): 4758-4768.

[21] Cattini S, Cassanelli D, Cecilia L D, et al. A procedure for the characterization and comparison of 3-D LiDAR systems[J]. IEEE Transactions on Instrumentation and Measurement, 2021, 70: 7002110.

[22] Li D, Xu L J, Xie X H, et al. Co-path full-waveform LiDAR for detection of multiple along-path objects[J]. Optics and Lasers in Engineering, 2018, 111: 211-221.

[23] Liu C, Xu L J, Si L, et al. A robust deconvolution method of airborne LiDAR waveforms for dense point clouds generation in forest[J]. IEEE Transactions on Geoscience and Remote Sensing, 2022, 60: 5700314.

[24] 单聪淼, 孙华燕, 赵延仲, 等. 相干高斯光束通过卡塞格伦镜头反射光的时间分布特性[J]. 中国激光, 2017, 44(12):

1205001.

Shan C M, Sun H Y, Zhao Y Z, et al. Temporal distribution characteristics of reflection light of coherent Gaussian beams passing through Cassegrain lens[J]. Chinese Journal of Lasers, 2017, 44(12): 1205001.

[25] Li D, Xu L J, Li X L, et al. Asymmetrical-Gaussian-model-based laser echo detection[J]. IEEE Sensors Journal, 2019, 19(10): 3797-3806.

[26] Li X L, Li Y Y, Xie X H, et al. Lab-built terrestrial laser scanner self-calibration using mounting angle error correction [J]. Optics Express, 2018, 26(11): 14444-14460.

[27] 徐昇凌, 杨琦, 杨开发, 等. 点云质量评价挑战与关键技术研究 [J]. 中国传媒大学学报(自然科学版), 2021, 28(5): 11-21.
Xu Y L, Yang Q, Yang K F, et al. Challenges and key technologies of point cloud quality assessment [J]. Journal of Communication University of China (Science and Technology), 2021, 28(5): 11-21.

[28] Alexiou E, Ebrahimi T, Bernardo M V, et al. Point cloud subjective evaluation methodology based on 2D rendering [C] // 2018 Tenth International Conference on Quality of Multimedia Experience (QoMEX), May 29-June 1, 2018, Cagliari, Italy. New York: IEEE Press, 2018: 132-137.

[29] MPEG 3DG. Evaluation criteria for PCC (point cloud compression): ISO/IEC MPEG N16332[S]. Geneva: ISO/IEC, 2016.

[30] Meynet G, Digne J, Lavoué G. PC-MSDM: a quality metric for 3D point clouds[C]//2019 Eleventh International Conference on Quality of Multimedia Experience (QoMEX), June 5-7, 2019, Berlin, Germany. New York: IEEE Press, 2019.

[31] Viola I, Subramanyam S, Cesar P. A color-based objective quality metric for point cloud contents [C] // 2020 Twelfth International Conference on Quality of Multimedia Experience (QoMEX), May 26-28, 2020, Athlone, Ireland. New York: IEEE Press, 2020.

[32] 马聪聪, 李松, 曹菁菁, 等. 基于法向量和密度的点云特征点提取问题研究[J]. 计算机应用与软件, 2020, 37(5): 256-260, 292.
Ma C C, Li S, Cao J J, et al. Feature points extraction of point cloud based on normal vector and density [J]. Computer Applications and Software, 2020, 37(5): 256-260, 292.

[33] Crespo-Peremarch P, Fournier R A, Nguyen V T, et al. A comparative assessment of the vertical distribution of forest components using full-waveform airborne, discrete airborne and discrete terrestrial laser scanning data[J]. Forest Ecology and Management, 2020, 473: 118268.

[34] Jansson J P, Koskinen V, Mantyniemi A, et al. A multichannel high-precision CMOS time-to-digital converter for laser-scanner-based perception systems [J]. IEEE Transactions on Instrumentation and Measurement, 2012, 61(9): 2581-2590.

[35] Seo H, Yoon H, Kim D, et al. Direct TOF scanning LiDAR sensor with two-step multievent histogramming TDC and embedded interference filter [J]. IEEE Journal of Solid-State Circuits, 2021, 56(4): 1022-1035.

[36] Xie W J, Wang Y, Chen H C, et al. 128-channel high-linearity resolution-adjustable time-to-digital converters for LiDAR applications: software predictions and hardware implementations [J]. IEEE Transactions on Industrial Electronics, 2022, 69(4): 4264-4274.

[37] Magruder L A, Neuenschwander A L, Marmillion S P, et al. Obstruction detection comparison of small-footprint full-waveform and discrete return lidar [J]. Proceedings of SPIE, 2010, 7684: 768410.

[38] RIEGL. Ultra high performance 3D laser scanner[EB/OL]. (2019-11-22) [2022-04-15]. http: // products. rieglusa. com/ Asset/Datasheet-RIEGL-VZ-400i-1.pdf.

[39] Azadbakht M, Fraser C S, Khoshelham K. A sparsity-based regularization approach for deconvolution of full-waveform airborne lidar data[J]. Remote Sensing, 2016, 8(8): 648.

[40] Li D, Liu M L, Ma R, et al. An 8-ch LIDAR receiver based on TDC with multi-interval detection and real-time in situ calibration [J]. IEEE Transactions on Instrumentation and Measurement, 2020, 69(7): 5081-5090.

[41] Xie X H, Xu L J, Wang Z N, et al. Real-time in situ laser ranging based on online echo waveform fitting[J]. IEEE Sensors Journal, 2019, 19(20): 9255-9262.

[42] Niclass C, Rochas A, Besse P A, et al. Design and characterization of a CMOS 3-D image sensor based on single photon avalanche diodes [J]. IEEE Journal of Solid-State Circuits, 2005, 40(9): 1847-1854.

[43] Niclass C, Favi C, Kluter T, et al. A 128×128 single-photon image sensor with column-level 10-bit time-to-digital converter array[J]. IEEE Journal of Solid-State Circuits, 2008, 43(12): 2977-2989.

[44] Niclass C, Soga M, Matsubara H, et al. A 0.18-μm CMOS SoC for a 100-m-range 10-frame/s 200×96-pixel time-of-flight depth sensor[J]. IEEE Journal of Solid-State Circuits, 2014, 49(1): 315-330.

[45] Hutchings S W, Johnston N, Gyongy I, et al. A reconfigurable 3-D-stacked SPAD imager with in-pixel histogramming for flash LIDAR or high-speed time-of-flight imaging[J]. IEEE Journal of Solid-State Circuits, 2019, 54(11): 2947-2956.

[46] Zhang C, Lindner S, Antolović I M, et al. A 30-frames/s, 252 ×144 SPAD flash LiDAR with 1728 dual-clock 48.8-ps TDCs, and pixel-wise integrated histogramming[J]. IEEE Journal of Solid-State Circuits, 2019, 54(4): 1137-1151.

[47] Yoshioka K, Kubota H, Fukushima T, et al. A 20-ch TDC/ADC hybrid architecture LiDAR SoC for 240×96 pixel 200-m range imaging with smart accumulation technique and residue quantizing SAR ADC[J]. IEEE Journal of Solid-State Circuits, 2018, 53(11): 3026-3038.

[48] Kondo S, Kubota H, Katagiri H, et al. An automotive LiDAR SoC for 240×192-pixel 225-m-range imaging with a 40-channel 0.0036-mm^2 voltage/time dual-data-converter-based AFE[J]. IEEE Journal of Solid-State Circuits, 2020, 55(11): 2866-2877.

[49] 朱世贤, 赵毅强, 叶茂, 等. 大动态范围激光雷达回波信号饱和处理算法[J]. 光子学报, 2018, 47(12): 1228003.
Zhu S X, Zhao Y Q, Ye M, et al. Saturated echo signal algorithm for wide dynamic range lidar [J]. Acta Photonica Sinica, 2018, 47(12): 1228003.

[50] Liu Y, Zhu J J, Roberts N, et al. Recovery of saturated signal waveform acquired from high-energy particles with artificial neural networks[J]. Nuclear Science and Techniques, 2019, 30(10): 148.

[51] Wang Z N, Xu L J, Li D, et al. Online multi-target laser ranging using waveform decomposition on FPGA [J]. IEEE Sensors Journal, 2021, 21(9): 10879-10889.

[52] 梁敏, 马凯. 基于高斯滤波的回波信号去噪方法的研究[J]. 测绘与空间地理信息, 2017, 40(1): 40-42.
Liang M, Ma K. Study on the method of echo signal denoising based on Gauss filter [J]. Geomatics & Spatial Information Technology, 2017, 40(1): 40-42.

[53] Schafer R W. What is a Savitzky-Golay filter?[J]. IEEE Signal Processing Magazine, 2011, 28(4): 111-117.

[54] Li X L, Zhang Z X, Xie X H, et al. A multi-target on-line ranging method based on matrix sparsification and a division-free Gauss-Jordan solver[J]. Measurement Science and Technology, 2021, 32(9): 095207.

[55] Babu C N, Reddy B E. A moving-average filter based hybrid ARIMA-ANN model for forecasting time series data [J]. Applied Soft Computing, 2014, 23: 27-38.

[56] Iqbal I A, Dash J, Ullah S, et al. A novel approach to estimate canopy height using ICESat/GLAS data: a case study in the New Forest National Park, UK[J]. International Journal of Applied Earth Observation and Geoinformation, 2013, 23: 109-118.

[57] Zhao X L, Xia H, Zhao J H, et al. Adaptive wavelet threshold

denoising for bathymetric laser full-waveforms with weak bottom returns［J］. IEEE Geoscience and Remote Sensing Letters, 2022, 19: 1503505.

[58] Song Y, Li H P, Zhai G J, et al. Comparison of multichannel signal deconvolution algorithms in airborne LiDAR bathymetry based on wavelet transform［J］. Scientific Reports, 2021, 11: 16988.

[59] 何亮. 小光斑 ALS 全波形数据处理技术研究［D］. 成都: 电子科技大学, 2015.
He L. Research on small-footprint ALS full-waveform data processing technology［D］. Chengdu: University of Electronic Science and Technology of China, 2015.

[60] 刘俊, 姚予木, 李培楠, 等. 激光测高卫星全波形回波数据的参数优化小波降噪［J］. 中国激光, 2021, 48(23): 2310001.
Liu J, Yao Y M, Li P N, et al. Parameter optimization wavelet denoising algorithm for full-waveforms data of laser altimetry satellite［J］. Chinese Journal of Lasers, 2021, 48 (23): 2310001.

[61] Huang N E, Shen Z, Long S R, et al. The empirical mode decomposition and the Hilbert spectrum for nonlinear and non-stationary time series analysis［J］. Proceedings of the Royal Society of London Series A: Mathematical, Physical and Engineering Sciences, 1998, 454(1971): 903-995.

[62] Cheng X, Mao J D, Li J, et al. An EEMD-SVD-LWT algorithm for denoising a lidar signal［J］. Measurement, 2021, 168: 108405.

[63] Wu Z H, Huang N E. Ensemble empirical mode decomposition: a noise-assisted data analysis method［J］. Advances in Adaptive Data Analysis, 2009, 1(1): 1-41.

[64] Boudraa A O, Cexus J C. EMD-based signal filtering［J］. IEEE Transactions on Instrumentation and Measurement, 2007, 56 (6): 2196-2202.

[65] Zhang Z J, Liu X F, Shu R, et al. A novel noise reduction method for space-borne full waveforms based on empirical mode decomposition［J］. Optik, 2020, 202: 163581.

[66] Dragomiretskiy K, Zosso D. Variational mode decomposition ［J］. IEEE Transactions on Signal Processing, 2014, 62(3): 531-544.

[67] Hua T, Dai K R, Zhang X J, et al. Optimal VMD-based signal denoising for laser radar via Hausdorff distance and wavelet transform［J］. IEEE Access, 2019, 7: 167997-168010.

[68] Qi B L, Yang G H, Guo D B, et al. EMD and VMD-GWO parallel optimization algorithm to overcome lidar ranging limitations［J］. Optics Express, 2021, 29(2): 2855-2873.

[69] Li X L, Luo P. Boosting ranging performance of LiDAR using multi-pulse coherent average［J］. IEEE Sensors Journal, 2019, 19(15): 6270-6278.

[70] 王婷. EMD 算法研究及其在信号去噪中的应用［D］. 哈尔滨: 哈尔滨工程大学, 2010: 79-87.
Wang T. Research on EMD algorithm and its application in signal denoising［D］. Harbin: Harbin Engineering University, 2010: 79-87.

[71] 丁红波, 王珍珠, 刘东. 激光雷达信号去噪方法的对比研究［J］. 光学学报, 2021, 41(24): 2401001.
Ding H B, Wang Z Z, Liu D. Comparison of de-noising methods of LiDAR signal［J］. Acta Optica Sinica, 2021, 41 (24): 2401001.

[72] 王振华, 刘晓丹, 刘向锋. GLAS 全波形数据的小波与经验模态分解降噪［J］. 激光与光电子学进展, 2021, 58(23): 2328001.
Wang Z H, Liu X D, Liu X F. Wavelet and empirical mode decomposition denoising for GLAS full waveform data［J］. Laser & Optoelectronics Progress, 2021, 58(23): 2328001.

[73] Jutzi B, Stilla U. Range determination with waveform recording laser systems using a Wiener filter［J］. ISPRS Journal of Photogrammetry and Remote Sensing, 2006, 61(2): 95-107.

[74] Nordin L. Analysis of waveform data from airborne laser scanner systems［D］. Luleå: Luleå University of Technology, 2006.

[75] Roncat A, Bergauer G, Pfeifer N. B-spline deconvolution for differential target cross-section determination in full-waveform laser scanning data［J］. ISPRS Journal of Photogrammetry and Remote Sensing, 2011, 66(4): 418-428.

[76] Wu J Y, van Aardt J A N, Asner G P. A comparison of signal deconvolution algorithms based on small-footprint LiDAR waveform simulation［J］. IEEE Transactions on Geoscience and Remote Sensing, 2011, 49(6): 2402-2414.

[77] Chauve A, Vega C, Durrieu S, et al. Advanced full-waveform lidar data echo detection: assessing quality of derived terrain and tree height models in an alpine coniferous forest［J］. International Journal of Remote Sensing, 2009, 30(19): 5211-5228.

[78] Mountrakis G, Li Y G. A linearly approximated iterative Gaussian decomposition method for waveform LiDAR processing ［J］. ISPRS Journal of Photogrammetry and Remote Sensing, 2017, 129: 200-211.

[79] Guo K, Xu W X, Liu Y X, et al. Gaussian half-wavelength progressive decomposition method for waveform processing of airborne laser bathymetry［J］. Remote Sensing, 2017, 10(2): 35.

[80] Xie X H, Xu L J, Li X L, et al. Online Gauss-Newton-based parallel-pipeline method for real-time in-situ laser ranging［J］. IEEE Sensors Journal, 2020, 20(13): 7087-7096.

[81] Muralikrishnan B, Ferrucci M, Sawyer D, et al. Volumetric performance evaluation of a laser scanner based on geometric error model［J］. Precision Engineering, 2015, 40: 139-150.

[82] 卜禹铭, 杜小平, 曾朝阳, 等. 无扫描激光三维成像雷达研究进展及趋势分析［J］. 中国光学, 2018, 11(5): 711-727.
Bu Y M, Du X P, Zeng Z Y, et al. Research progress and trend analysis of non-scanning laser 3D imaging radar［J］. Chinese Optics, 2018, 11(5): 711-727.

[83] 亢甲杰, 张福民, 曲兴华. 激光雷达坐标测量系统的测角误差分析［J］. 激光技术, 2016, 40(6): 834-839.
Kang J J, Zhang F M, Qu X H. Angle measuring error analysis of coordinate measuring system of laser radar［J］. Laser Technology, 2016, 40(6): 834-839.

[84] Zhou Y, Lu Y F, Hei M, et al. Pointing error analysis of Risley-prism-based beam steering system［J］. Applied Optics, 2014, 53(25): 5775-5793.

[85] Brazeal R G, Wilkinson B E, Hochmair H H. A rigorous observation model for the Risley prism-based Livox Mid-40 lidar sensor［J］. Sensors, 2021, 21(14): 4722.

[86] Guo D B, Wang C H, Qi B L, et al. A study of correction to the point cloud distortion based on MEMS LiDAR system ［J］. Applied Sciences, 2021, 11(5): 2418.

[87] 缪新, 李航锋, 张运海, 等. MEMS 振镜扫描共聚焦图像畸变机理分析及校正［J］. 红外与激光工程, 2021, 50(2): 20200206.
Miao X, Li H F, Zhang Y H, et al. Analysis and correction of image distortion in MEMS galvanometer scanning confocal system［J］. Infrared and Laser Engineering, 2021, 50 (2): 20200206.

[88] Spollard J T, Gozzard D R, Roberts L E, et al. Towards solid-state beam steering using a 7-emitter 1550 nm optical phased array［J］. Proceedings of SPIE, 2019, 10910: 109101P.

[89] Zhang W C, Li L J, Chen W. A chaotic stochastic parallel gradient descent algorithm for fast phase correction of optical phased array［J］. Proceedings of SPIE, 2019, 11209: 1120956.

[90] 唐辉. 光学相控阵(OPA)光相位控制性能测试系统的研制［D］. 长春: 吉林大学, 2021.
Tang H. Development of optical phase control performance test system for optical phased array (OPA)［D］. Changchun: Jilin University, 2021.

[91] Lichti D D. Ray-tracing method for deriving terrestrial laser scanner systematic errors［J］. Journal of Surveying Engineering, 2017, 143(2): 06016005.

[92] Abbas M A, Lichti D D, Chong A K, et al. An on-site approach for the self-calibration of terrestrial laser scanner ［J］. Measurement, 2014, 52: 111-123.

[93] Pejić M, Ogrizović V, Božić B, et al. A simplified procedure of

metrological testing of the terrestrial laser scanners［J］. Measurement, 2014, 53: 260-269.

［94］ Li X L, Li Y Y, Xie X H, et al. Terrestrial laser scanner autonomous self-calibration with no prior knowledge of point-clouds［J］. IEEE Sensors Journal, 2018, 18(22): 9277-9285.

［95］ Holst C, Schunck D, Nothnagel A, et al. Terrestrial laser scanner two-face measurements for analyzing the elevation-dependent deformation of the Onsala Space Observatory 20-m radio telescope's main reflector in a bundle adjustment［J］. Sensors, 2017, 17(8): 1833.

［96］ Wang L, Muralikrishnan B, Rachakonda P, et al. Determining geometric error model parameters of a terrestrial laser scanner through two-face, length-consistency, and network methods［J］. Measurement Science & Technology, 2017, 28(6): 065016.

［97］ 官云兰, 程效军, 詹新武, 等. 地面三维激光扫描仪系统误差标定［J］. 测绘学报, 2014, 43(7): 731-738.
Guan Y L, Cheng X J, Zhan X W, et al. Research on systematic errors calibration of terrestrial laser scanner［J］. Acta Geodaetica et Cartographica Sinica, 2014, 43(7): 731-738.

［98］ Shi S D, Muralikrishnan B, Sawyer D. Terrestrial laser scanner calibration and performance evaluation using the network method［J］. Optics and Lasers in Engineering, 2020, 134: 106298.

［99］ 张毅, 闫利, 杨红, 等. 地面三维激光扫描的系统误差模型研究［J］. 测绘通报, 2012, 16(1): 16-19.
Zhang Y, Yan L, Yang H, et al. Research on systematic error model of terrestrial laser scanning［J］. Bulletin of Surveying and Mapping, 2012, 16(1): 16-19.

［100］ Morales J, Plaza-Leiva V, Mandow A, et al. Analysis of 3D scan measurement distribution with application to a multi-beam lidar on a rotating platform［J］. Sensors, 2018, 18(2): 395.

［101］ 覃兴胜, 李晓欢, 唐欣, 等. 基于标定板关键点的激光雷达与相机外参标定方法［J］. 激光与光电子学进展, 2022, 59(4): 0428001.
Qin X S, Li X H, Tang X, et al. Extrinsic calibration method of lidar and camera based on key points of calibration board［J］. Laser & Optoelectronics Progress, 2022, 59(4): 0428001.

［102］ Chan T O, Lichti D D. Automatic in situ calibration of a spinning beam LiDAR system in static and kinematic modes［J］. Remote Sensing, 2015, 7(8): 10480-10500.

［103］ Bastos D, Monteiro P P, Oliveira A S R, et al. An overview of LiDAR requirements and techniques for autonomous driving［C］// 2021 Telecoms Conference (ConfTELE), February 11-12, 2021, Leiria, Portugal. New York: IEEE Press, 2021.

［104］ Yang F H. Analysis of lidar technology development based on autonomous driving competition［C］// 2021 International Conference of Optical Imaging and Measurement (ICOIM), August 27-29, 2021, Xi'an, China. New York: IEEE Press, 2021: 170-173.

［105］ Li Y, Ibanez-Guzman J. Lidar for autonomous driving: the principles, challenges, and trends for automotive lidar and perception systems［J］. IEEE Signal Processing Magazine, 2020, 37(4): 50-61.

［106］ Tang J, Yellepeddi A, Demirtas S, et al. Tracking to improve detection quality in lidar for autonomous driving［C］//ICASSP 2020—2020 IEEE International Conference on Acoustics, Speech and Signal Processing, May 4-8, 2020, Barcelona, Spain. New York: IEEE Press, 2020: 2683-2687.

［107］ Yoo H W, Druml N, Brunner D, et al. MEMS-based lidar for autonomous driving［J］. E & I Elektrotechnik Und Informationstechnik, 2018, 135(6): 408-415.

［108］ Takai I, Matsubara H, Soga M, et al. Single-photon avalanche diode with enhanced NIR-sensitivity for automotive LIDAR systems［J］. Sensors, 2016, 16(4): 459.

［109］ 欧阳波. 基于三维点云的动态目标位姿估计［D］. 长沙: 国防科学技术大学, 2015: 6-7.
Ouyang B. Dynamic pose estimation based on 3D point cloud［D］. Changsha: National University of Defense Technology,

2015: 6-7.

［110］ Nimelman M, Tripp J, Bailak G, et al. Spaceborne scanning lidar system (SSLS)［J］. Proceedings of SPIE, 2005, 5798: 73-82.

［111］ Christian J, Hinkel H, Maguire S, et al. The sensor test for Orion RelNav risk mitigation (STORRM) development test objective［C］// AIAA Guidance, Navigation, and Control Conference, August 8-11, 2011, Portland, Oregon. Virginia: AIAA Press, 2011: 6260.

［112］ 胡军, 解永春, 张昊, 等. 神舟八号飞船交会对接制导、导航与控制系统及其飞行结果评价［J］. 空间控制技术与应用, 2011, 37(6): 1-5, 13.
Hu J, Xie Y C, Zhang H, et al. Shenzhou-8 spacecraft guidance navigation and control system and flight result evaluation for rendezvous and docking［J］. Aerospace Control and Application, 2011, 37(6): 1-5, 13.

［113］ 解永春, 张昊, 胡军, 等. 神舟飞船交会对接自动控制系统设计［J］. 中国科学: 技术科学, 2014, 44(1): 12-19.
Xie Y C, Zhang H, Hu J, et al. Automatic control system design of Shenzhou spacecraft for rendezvous and docking［J］. Scientia Sinica (Technologica), 2014, 44(1): 12-19.

［114］ Christian J A, Cryan S. A survey of LIDAR technology and its use in spacecraft relative navigation［C］// AIAA Guidance, Navigation, and Control (GNC) Conference, August 19-22, 2013, Boston, MA, USA. Virginia: AIAA Press, 2013: 4641.

［115］ 徐阳, 马琳, 刘涛, 等. 嫦娥五号月球轨道交会对接制导、导航与控制系统［J］. 中国科学: 技术科学, 2021, 51(7): 788-798.
Xu Y, Ma L, Liu T, et al. Chang'e-5 guidance navigation and control system for rendezvous and docking in lunar orbit［J］. Scientia Sinica (Technologica), 2021, 51(7): 788-798.

［116］ 黄翔宇, 张洪华, 王大轶, 等. "嫦娥三号"探测器软着陆自主导航与制导技术［J］. 深空探测学报, 2014, 1(1): 52-59.
Huang X Y, Zhang H H, Wang D Y, et al. Autonomous navigation and guidance for Chang'e-3 soft landing［J］. Journal of Deep Space Exploration, 2014, 1(1): 52-59.

［117］ 张洪华, 梁俊, 黄翔宇, 等. 嫦娥三号自主避障软着陆控制技术［J］. 中国科学: 技术科学, 2014, 44(6): 559-568.
Zhang H H, Liang J, Huang X Y, et al. Autonomous hazard avoidance control for Chang'e-3 soft landing［J］. Scientia Sinica (Technologica), 2014, 44(6): 559-568.

［118］ 舒嵘, 徐卫明, 黄庚华. 用于行星导航和软着陆的激光雷达系统［C］//中国宇航学会深空探测技术专业委员会第十届学术年会论文集. 北京: 中国宇航学会, 2013: 502-505.
Shu R, Xu W M, Huang G H. Lidar systems for planetary navigation and soft landing［C］//10th Annual Conference of Deep Space Exploration Technology Committee. Beijing: Chinese Society of Astronautics, 2013: 502-505.

［119］ Mizuno T, Kase T, Shiina T, et al. Development of the laser altimeter (LIDAR) for Hayabusa2［J］. Space Science Reviews, 2017, 208(1): 33-47.

［120］ Amzajerdian F, Roback V E, Bulyshev A E, et al. Imaging flash LIDAR for safe landing on solar system bodies and spacecraft rendezvous and docking［J］. Proceedings of SPIE, 2015, 9465: 946502.

［121］ Schindhelm E, Rohrschneider R, Roark S, et al. A scanning LIDAR system for active hazard detection and avoidance during landing on Europa［C］// 2018 IEEE Aerospace Conference, March 3-10, 2018, Big Sky, MT, USA. New York: IEEE Press, 2018.

［122］ Williams B, Antreasian P, Carranza E, et al. OSIRIS-Rex flight dynamics and navigation design［J］. Space Science Reviews, 2018, 214(4): 69.

［123］ 刘旺旺, 李茂登, 李涛, 等. 天问一号探测器火星着陆自主避障技术设计与验证［J］. 宇航学报, 2022, 43(1): 46-55.
Liu W W, Li M D, Li T, et al. Design and qualification of hazard detection and avoidance system for Tianwen-1 Mars landing mission［J］. Journal of Astronautics, 2022, 43(1): 46-55.

Review on Key Technologies of Lightweight Type-Aware LiDAR

Li Xiaolu[*], Zhou Yier, Bi Tengfei, Yu Ruiqin, Wang Zining, Huang Jianbin, Xu Lijun[**]

School of Instrumentation Science and Opto-Electronics Engineering, Beihang University, Beijing 100191, China

Abstract

Significance　The lightweight type-aware light detection and ranging (LiDAR) is an active three-dimensional (3D) optical imaging technology used for environment perception. Mounted on platforms such as vehicles and aircrafts, the type-aware LiDAR performs as the eye to capture and process environmental information, providing real-time and accurate 3D data for target detection, identification and decision making. Compared with the traditional surveying and mapping LiDAR, the type-aware LiDAR has the advantages of smaller volume, larger amount of data, higher transmission rate and higher-resolution 3D imaging. As the demand of 3D sensing grows, the lightweight type-aware LiDAR technology becomes one of the hotspots in the future development. The type-aware LiDAR is mainly applied in the fields of aerospace exploration and autonomous driving. To meet the requirements of miniaturization and intelligence, the key technologies of type-aware LiDAR are developing toward lightweight system design. In this paper, the current key technologies and typical applications of lightweight type-aware LiDAR are summarized, and the development trend of key technologies is forecasted.

Progress　Firstly, the integration-level LiDAR has been greatly contributed by the development of fiber and semiconductor lasers, single photon detector, and micro-electro-mechanical system (MEMS) and optical phased array (OPA) laser scanner. Fiber laser has been employed for aerospace application with adjustable repetition rate of 5−50 kHz. With an inherently safer wavelength for autonomous driving application, vertical cavity surface emitting laser (VCSEL) of 1550 nm has better carrier confinement than semiconductor laser of 905 nm. Single photon avalanche diode (SPAD) array with hundreds of pixels has been developed for 3D imaging on femtosecond magnitude. The 4 pixel × 4 pixel silicon photomultiplier (SiPM) has been developed to capture light intensity information, whose single pixel is composed of 100 SPADs (Fig. 1). To facilitate integration, scan unit of type-aware LiDAR is gradually developing from the traditional multi-beam mechanical scanning type to MEMS, OPA, and flash LiDAR (Table 1), and the ranging system is developing toward system on chip (SoC) technology.

Secondly, the ranging performance of LiDAR has a significant influence on the quality of point cloud, which is elaborated from two aspects of ranging system and ranging algorithm. The ranging system can be categorized as time-to-digital converter (TDC) and analogue-to-digital converter (ADC) according to the implementation schemes of time discrimination. In order to miniaturize the ranging system, the TDC/ADC hybrid SoC is designed to achieve long-range detection (Fig. 4). Toshiba has developed a 40-channel LiDAR SoC with a ranging error less than 0.25% and a distance ranging from 25 m to 225 m. Subsequently, the ranging algorithms for saturated, weak, and multiple echo waveforms are summarized separately. The selection of algorithms depends on the signal situation and application condition. With the recent developments, SoC is becoming the mainstream form of ranging system and the ranging algorithms need to evolve for processing more complicated signal.

Thirdly, the research status of pointing error correction of type-aware LiDAR is introduced, including the correction of scanning mechanism internal errors and system installation errors. The scanning mechanism internal errors can be eliminated by correction function obtained from mechanism analysis (Fig. 6), which is elaborated in various scanning mechanism of prism, MEMS and OPA. The system installation error is reduced by modeling the difference between the actual laser path and the ideal path, as well as adopting model optimization methods include network method, two-face method and length-consistency method. The future research of the pointing error correction needs more generalization and process standardization.

Fourthly, lightweight type-aware LiDAR has been employed in versatile applications. For autonomous driving application, low cost and potential for integration are required (Fig. 9). Mechanical (ranging 100−500 m, accuracy 2−7 cm) and hybrid solid-state scanning systems (ranging 150−500 m, accuracy up to 1 cm) are currently the prevailing types of LiDAR loaded on autonomous vehicles. As for space application, the flash LiDAR is commonly utilized in space rendezvous and hazard avoidance tasks due to its high directivity, high resolution and high precision (Table 3 and Table 4).

Prospects　Lightweight type-aware LiDAR has become the development frontier and research hotspot in the field of intelligent sensors. In the past decade, hybrid-solid MEMS LiDAR as a mature product has sprung up. As the integrated chip technology fast grows, SoC technology perhaps becomes a mainstream solution to performance improvements of lightweight type-aware LiDAR with compactness, high resolution and high speed. In the future, the on-chip technology

integrated with signal processing algorithm, state-solid scanning mechanism combined with universal correction method, and mutual promotion of technologies between civil and aerospace applications, will motivate the development of lightweight type-aware LiDAR.